

## Interactions of excited ( $n = 3$ ) and ground-state helium atoms: Potential curves and inelastic processes\*

W. J. Steets<sup>†</sup> and N. F. Lane

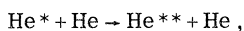
Physics Department, Rice University, Houston, Texas 77001

(Received 19 November 1974)

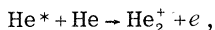
Adiabatic potential-energy curves have been calculated for the interaction of several  $n = 3$  triplet states of helium with ground-state helium. Mechanisms for excitation-transfer in collisions of  $3^3S$  and  $3^3P$  with ground-state atoms are suggested by the results of these calculations. A deexcitation cross section corresponding to  $3^3S \rightarrow 2^3P$  excitation-transfer has been calculated using the Stueckelberg-Landau-Zener approximation and is consistent with existing measurements. The existence of a small hump in the potential curve causes the cross section to decrease rapidly at low energies. Thus, a strong temperature dependence of effective cross sections is expected. A possible mechanism for associative ionization is also discussed.

### I. INTRODUCTION

In a slow collision between an excited and a ground-state helium atom, two inelastic processes are possible. These are nonresonant excitation transfer



where the excitation may end up on either of the atoms, and associative ionization



where the molecular ion may be formed in any of a number of vibrational and rotational states. These reactions have been observed in gas discharges and afterglows.<sup>1,2</sup>

As a first step in understanding these processes, we have calculated adiabatic potential-energy curves for several  $^3\Pi_u$ ,  $^3\Sigma_u^+$ , and  $^3\Sigma_g^+$  states of  $\text{He}_2$  using the valence-bond configuration-interaction method. We have used these potential curves and the Stueckelberg-Landau-Zener approximation to compute cross sections for the excitation-transfer processes  $3^3S \rightarrow 2^3P$ . In addition, several different representations (nonadiabatic) of the electronic wave function have been studied to suggest a mechanism for associative ionization.

In Secs. II and III, the method of calculation and the general nature of the molecular states are discussed. In Sec. IV our results for the  $^3\Sigma_u^+$  and  $^3\Sigma_g^+$  excited states involved in the collision processes are considered. The possible existence of a diabatic state leading to associative ionization is discussed in Sec. V. The collision processes themselves are considered in Sec. VI.

### II. CALCULATION OF ENERGIES AND WAVE FUNCTIONS

The electronic wave functions used in the present study were of the form

$$\Psi(\vec{r}_e, R) = \sum_j c_j \Psi_j(\alpha; \vec{r}_e, R), \quad (1)$$

where  $\vec{r}_e$  represents all of the electronic coordinates collectively, and  $R$  is the internuclear separation. Each configuration function  $\Psi_j(\alpha; \vec{r}_e, R)$  is a sum of Slater determinants constructed to be eigenfunctions of the symmetry operations of the molecule and of the total-spin operators  $S^2$  and  $S_z$ . The  $\alpha$  denotes a set of orbital exponents contained in the elementary basis functions which are used to construct the Slater determinants. The elementary basis functions are Slater-type orbitals (STO) centered on either nucleus  $A$  or  $B$ .

Five types of configuration wave functions are used in these calculations. These are shown in Table I. The notation for the configurations is that of Gupta and Matsen<sup>3</sup> in which the orbitals within parentheses are spin paired and the orbitals in square brackets are used to construct fully symmetrized configurations. For the  $^3\Pi_u$  and  $^3\Sigma_u^+$  states, the ionic-covalent form was chosen, whereas for the  $^3\Sigma_g^+$  states, the covalent form alone was used. In these calculations, we sought to represent several excited states of a particular symmetry equally well. This was achieved by using configurations formed from three core atomic orbitals and one excited-atom orbital. Our interest was primarily in states dissociating to the  $n = 3$  atomic states. Hence, the orbital exponents were chosen by partially optimizing the separated-atom energies of these states. The orbital exponents were not varied with internuclear separation.

As an indication of the accuracy of this procedure, we have compared the calculated and observed effective quantum numbers for these states. As may be seen in Table II, the agreement is generally good. The poorest results are for  $s\sigma$  states, where the interaction of the excited orbital with the core is greatest and, thus, where we would ex-

TABLE I. Wave functions.

Ionic
$\Psi = [1s'_a(1s_b1s_b)]$
Covalent
$\Psi = \sum_i C_i [1s'_a \varphi_{ai}(1s_b1s_b)]$
Ionic-covalent
$\Psi = \sum_i \{C_i [1s'_a \varphi_{ai}(1s_b1s_b)] + D_i [1s'_a \varphi_{bi}(1s_b1s_b)]\}$
A core
$\Psi = \sum_i C_i \{[1s'_b \varphi_{ai}(1s_a1s_a)] - [1s'_a \varphi_{ai}(1s_b1s_b)]\}$
B core
$\Psi = \sum_i C_i \{[1s'_b \varphi_{ai}(1s_b1s_b)] + [1s'_a \varphi_{ai}(1s_b1s_b)]\}$

pect the simple representation of the core to be most in error.

### III. EXCITED STATES OF He<sub>2</sub>

#### A. He<sub>2</sub><sup>+</sup> ion

Our goal in the work is to calculate the *relative* positions of the potential-energy curves as accurately as possible for several excited states. The excited-state wave functions are constructed with a very simple representation of the He<sub>2</sub><sup>+</sup> ion core. More extensive configuration interaction is allowed among the excited orbitals themselves. The dominant contribution to the absolute error arises, however, from the overly simple representation of the core. In order to estimate this error, we compare the He<sub>2</sub><sup>+</sup>(<sup>2</sup>Σ<sub>u</sub><sup>+</sup>) potential-energy curve calculated from the single configuration

wave function of the form given in Table I with that of Reagan, Browne, and Matsen<sup>5</sup> who used a 26-configuration wave function. For intermediate internuclear separations the difference between the two curves is approximately independent of  $R$ . As a further check, we have compared our potential curve for the lowest He<sub>2</sub><sup>3</sup>Π<sub>u</sub> states with that calculated by Gupta and Matsen.<sup>3</sup> Again, there is almost a constant difference between the two curves, and this difference is within 0.003 a.u. of that observed between the two ion curves. This comparison suggests that we may approximately correct the excited-state curves by simply subtracting the difference in the ion potential energy curves at each  $R$ . This provides ion-core "adjusted" potentials which compare better with the results of other calculations and with experiment.

Again, it should be stressed that we do not seek highly accurate *ab initio* potential curves for excited states of He<sub>2</sub>. We wish to describe semi-quantitatively the relative behavior of potential curves for states important to inelastic processes involving  $n = 3$  helium atoms. We do not object to "adjusting" curves where the procedure is well defined and can be justified.

#### B. Description of the potential curves and wave functions

Since the excited states of He<sub>2</sub> are Rydberg states, the shapes of the potential curves near the equilibrium separation are largely determined by the potential curve of the He<sub>2</sub><sup>+</sup> ion core to which they are bound. The two lowest states of He<sub>2</sub><sup>+</sup> are the A<sup>2</sup>Σ<sub>u</sub><sup>+</sup> ("A core") and the B<sup>2</sup>Σ<sub>g</sub><sup>+</sup> ("B core"). The A<sup>2</sup>Σ<sub>u</sub><sup>+</sup> is stable with a dissociation energy of 2.47 eV. The B<sup>2</sup>Σ<sub>g</sub><sup>+</sup> is unstable with respect to dissociation of ground-state He and He<sup>+</sup>.

Recently Guberman and Goddard<sup>6</sup> have studied the singlet excited states of He<sub>2</sub> using the gener-

TABLE II. Quantum defects in triplet system.

State	Ionization energy (a.u.)	Calculated $n^*$	Calculated $\delta$	Experimental $n^*$ (Ref. 4)
2s	0.150 13	1.8249	0.1751	1.7885
3s	0.062 02	2.8394	0.1607	2.808
3pσ	0.104 96	2.1826	0.8174	2.1648
3dσ	0.058 14	2.9325	0.0675	2.9326
3dπ	0.057 24	2.9555	0.0445	2.9571
4s	0.033 74	3.8496	0.1504	3.8131
4pσ	0.047 84	3.2327	0.767 26	
4dσ	0.032 15	3.9436	0.0564	3.931
4dπ	0.031 94	3.9565	0.0435	3.956
4fσ	0.030 46	4.0515	-0.0515	
5pσ	0.027 71	4.2478	0.7522	
5dπ	0.020 44	4.9454	0.0541	4.95

alized-valence-bond (GVB) method. They discuss the behavior of their potential curves in terms of frozen-orbital (FO) configuration functions. These are single valence-bond configurations constructed from orbitals which do not change with  $R$ . These FO configurations have the property that, as  $R$  decreases, the single-configuration wave function approaches a Rydberg orbital on either an  $A$  or a  $B$  core. The configuration functions chosen by us and used in this work have the same property, viz.,

$$|nl_A 1s'_A 1s_B \bar{1}s_B| \pm |nl_B 1s'_B 1s_A \bar{1}s_A| \\ \underset{(R \rightarrow R_0)}{\sim} |nl_C (1s'_A 1s_B \bar{1}s_B \pm 1s'_B 1s_A \bar{1}s_A)|, \quad (2)$$

where  $nl_C$  is an STO with the same  $n$ ,  $l$ , and variational parameter  $\alpha$  as  $nl_A$  and  $nl_B$ , but which is centered at the midpoint of the two nuclei. Configuration wave functions constructed from the sum (difference) of these two determinants tend toward the product of the Rydberg orbital and the  $B$ -core ( $A$ -core) function.

This property of VB configuration wave functions allows us to predict the behavior of the energies of these configurations near the equilibrium separation. Since the configuration wave functions constructed from the sum of two determinants tend toward a  $B$  core, the corresponding potential curves are repulsive. Likewise, the configuration wave functions formed from the difference of two determinants tend toward an  $A$  core, and hence correspond to attractive potential curves. Taking into account the total inversion symmetry of the configuration, we have the following rules<sup>6</sup> for single-configuration potential-energy curves corresponding to a Rydberg state  $nl$ .

(a) *Gerade symmetry*: (i) Even- $l$  configurations are repulsive, (ii) odd- $l$  configurations are attractive.

(b) *Ungerade symmetry*: (i) Even- $l$  configurations are attractive, (ii) odd- $l$  configurations are repulsive.

These single-configuration rules are particularly useful in interpreting features of the complicated potential curves which arise in the multiconfiguration calculations.

There are two fundamental types of interactions which can explain unusual features in the potential curves such as the humps which are often found in the  $\text{He}_2$  system. The first of these is an exchange interaction caused by the repulsion of an electron in an excited orbital on one atom by the electrons in the closed-shell ground state on the other atom. This effect has been explained in some detail by Guberman and Goddard.<sup>6</sup> The interaction varies with the probability density of the excited orbital

in the region of the ground-state atom, and is most important for  $\Sigma$  states. The second type of interaction is due to the mutual perturbation of several configurations. There are two cases to be distinguished. The first is usually referred to as an avoided crossing and is caused by the interaction of configurations tending toward different ion cores. The second involves the interaction of configurations, usually over an extended region where the single-configuration potential curves are nearly parallel. Instances of the second case occur more for large and small values of  $R$  than for intermediate values.

The avoided-crossing interactions are understood in terms of the behavior of the energies of single-configuration wave functions as described above. Because a single STO is used for each orbital in a determinant and because the orbital exponents are themselves determined by multiconfiguration-variational calculations on the separated-atom states, several configuration functions with the same  $l$  usually contribute to the electronic wave function for a single state at large  $R$ . As one goes to smaller  $R$ , the rapidly increasing energy of the  $B$ -core and rapidly decreasing energy of the  $A$ -core ion states, as compared to the spacing of the separated-atom energies, will force the potential curves of certain single-configuration functions to approach one another and eventually cross. The interaction of these configurations of the same symmetry prevents a crossing from actually occurring in the multiconfiguration curves, often resulting in a hump in the potential curve of the lower state, and sometimes a ripple in the upper curve.

The effects of the interaction of configurations with nearly parallel potential-energy curves depend on whether the interaction occurs at large or at small  $R$ . We first describe the large- $R$  case. As the principal quantum number of the excited states of He increases, the separation between adjacent angular momentum states generally decreases. States of  $\Sigma$  symmetry may be formed from all excited states. As  $R$  decreases, the energy levels of  $\Sigma$  states are perturbed by the exchange interaction. This exchange interaction mixes adjacent states when the energy separation is small. This interaction differs from the avoided-crossing interactions in that the initial relative position of the interacting states may be restored at smaller  $R$  where the exchange interaction is not important. This interaction may have the effect of reducing the perturbation due to the exchange interaction on the lower-state potential curve.

For small  $R$  the effects of the interaction of configurations with nearly parallel potential-energy curves are somewhat different. As the effective quantum number of the excited Rydberg states of

$\text{He}_2$  increases, the potential curves of adjacent states closely approach one another. The mixing of configurations of different  $l$  is very small in the vicinity of the equilibrium internuclear separation. In some instances it happens that, as  $R$  increases from its equilibrium value, the wave functions for two adjacent states appear reversed. This change occurs very abruptly, reflecting the very weak interaction between configurations of different  $l$  in the region.

To describe the behavior of the wave functions, it is desirable to have a quantitative measure of the contribution of a particular configuration. Since the single-configuration-state functions are not orthogonal, the squares of the expansion coefficients  $C_j$  in the free configuration-interaction (CI) wave functions are not true indicators of the contribution of a particular configuration. The "structure projections,"<sup>7</sup> defined by

$$P_j = C_j \sum_m S_{jm} C_m, \quad (3)$$

where  $S_{jm}$  are elements of the overlap matrix between single-configuration functions, are such indicators. The sum of the structure projections of single-configuration-state functions containing excited orbitals of the same  $l$  are useful in characterizing the complicated multiconfiguration wave function. We refer to these sums as "cumulative structure projections."

#### IV. POTENTIAL CURVES AND WAVE FUNCTIONS

In this section, we discuss in detail only those states of  $\text{He}_2$  which are used to explain the inelastic collisions  $3^3S \rightarrow 2^3P$  and  $3^3P \rightarrow 3^3S$ . These are the  $^3\Sigma_u^+$  ( $3s\sigma, 2p$ ) and  $^3\Sigma_u^+$  ( $3d\sigma, 3s$ ) states and for the second transition the  $^3\Sigma_g^+$  ( $5p\sigma, 3p$ ) states. The no-

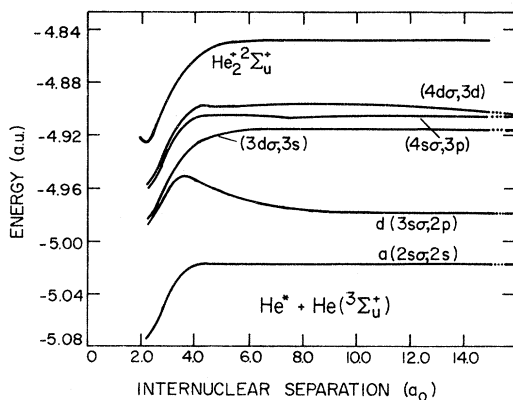


FIG. 1. Adiabatic potential curves at intermediate internuclear separations for the five lowest  $^3\Sigma_u^+$  states of  $\text{He}_2$  and the  $^2\Sigma_u^+$  ground state of  $\text{He}_2^+$ .

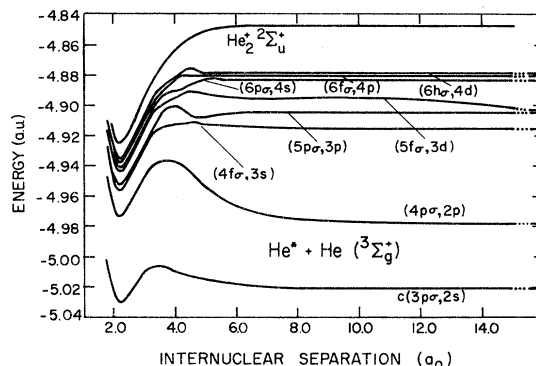


FIG. 2. Adiabatic potential curves at intermediate internuclear separations for the eight lowest  $^3\Sigma_g^+$  states of  $\text{He}_2$  and the  $^2\Sigma_u^+$  ground state of  $\text{He}_2^+$ .

tation of Guberman is used to denote the states.<sup>6</sup> The potential curves for the  $^3\Sigma_u^+$  and  $^3\Sigma_g^+$  states are shown in Figs. 1 and 2, respectively. In addition, the potential curves for several  $^3\Pi_u$  states are shown in Fig. 3.

#### A. $^3\Sigma_u^+$ ( $3s\sigma, 2p$ )

The potential curve for this state displays a large hump at  $3.68a_0$  with a magnitude of 0.0249 a.u., calculated from ion-core adjusted potentials. The origin of this hump in terms of the interaction of attractive and repulsive configuration-state functions is indicated by the cumulative structure projections for this state shown in Fig. 4. For large  $R$ , the repulsive  $p\sigma$  configuration-state functions are dominant in the wave function. Near the peak in the hump, the attractive  $d\sigma$  and  $s\sigma$  configurations strongly mix in, causing the adiabatic

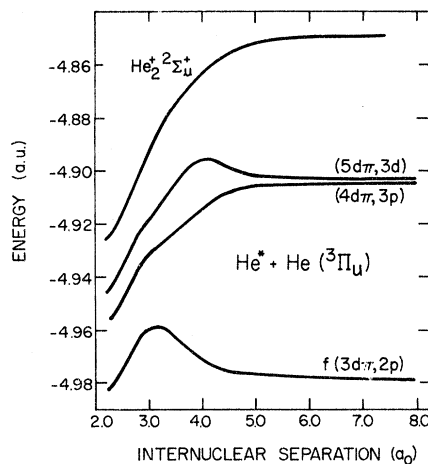


FIG. 3. Adiabatic potential curves at intermediate internuclear separations for the three lowest  $^3\Pi_u$  states of  $\text{He}_2$  and the  $^2\Sigma_u^+$  ground state of  $\text{He}_2^+$ .

potential curve to become attractive. The behavior of the wave function for the state at smaller  $R$  is discussed below.

#### B. ${}^3\Sigma_u^+(3d\sigma,3s)$

There is a small hump of 0.0009 a.u. near  $R = 10.0a_0$ . The location of this hump and the absence of crossing states suggest that the hump arises from the exchange interaction. The cumulative structure projections for the state are shown in Fig. 4. These indicate that there is little mixing of different configuration functions for  $R$  larger than  $2.75a_0$ . Between  $2.75$  and  $2.50a_0$ , the dominant configuration wave function abruptly changes from  $s\sigma$  to  $d\sigma$ . At the same separation the dominant configuration wave function for the  $(3s\sigma, 2p)$  state changes from  $d\sigma$  to  $s\sigma$ . There is, in effect, a crossing of two states. Ginter and Battino<sup>9</sup> have constructed potential curves for these states from spectroscopic data. They show the potential curves for these two states crossing near  $2.7a_0$ . We have interpolated the potential curves for these two states through the region of closest approach and find a crossing point of  $2.72a_0$ . We suggest this crossing as the mechanism for the  $3^3S - 2^3P$  excitation-transfer process.

#### C. ${}^3\Sigma_g^+(4f\sigma,3s)$

The potential curve for this state contains two small humps. The first maximum occurs in the vicinity of  $10a_0$  and has a magnitude of 0.00058 a.u. The location of this hump and the absence of possible crossing configurations suggest that this is also due to the exchange interaction. The second peak has a magnitude of 0.00216 a.u. and occurs at  $4.69a_0$ . The cumulative structure projections for this state are shown in Fig. 5. These indicate that the wave function consists almost entirely of  $s\sigma$ -configuration state functions for large  $R$ . In the

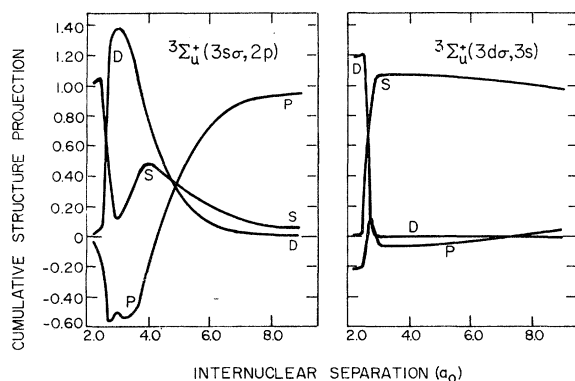


FIG. 4. Cumulative structure projections for the  $(3s\sigma, 2p)$  and  $(3d\sigma, 3s)$   ${}^3\Sigma_u^+$  states of  $\text{He}_2$ .

vicinity of the inner hump,  $p\sigma$  configurations are abruptly mixed in. This indicates a crossing of the repulsive  $s\sigma$  configurations and the attractive  $p\sigma$  configurations. Thus the inner hump is simply due to an avoided crossing. Between  $4.69$  and  $3.0a_0$ , the wave function retains its  $p\sigma$  character. Near  $3.0a_0$ , the  $p\sigma$  configurations are crossed by the  $f\sigma$  configurations. Both of these configurations are attractive so no hump occurs in the potential curve. The wave function continues to be dominated by the  $f\sigma$  configurations throughout the equilibrium region.

#### D. ${}^3\Sigma_g^+(5p\sigma,3p)$

The potential curve for this state has a hump of 0.00057 a.u. peaking near  $10a_0$ . The position of the hump suggests that it is due to the exchange interaction. The cumulative structure projections, however, indicate that the adjacent  $d\sigma$  configurations are mixed into the wave function. Since the wave function regains its  $p\sigma$  character at intermediate values of  $R$ , this interaction cannot be considered a simple crossing of potential curves in the usual sense.

As  $R$  decreases, the attractive  $p\sigma$  configurations cause the potential curve to fall to a minimum of 0.00044 a.u. (with respect to the separated-atoms energies) at  $4.68a_0$ . The cumulative structure projections indicate that this feature is due to an avoided crossing with the lower  $(4f\sigma, 3s)$  state. It is this crossing which we suggest is primarily responsible for the  $3^3P - 3^3S$  excitation transfer. A second maxima of 0.00164 a.u. occurs near  $3.92a_0$  due to an interaction with attractive  $f$ -type configurations. Finally there is an abrupt transition at  $3.0a_0$  where the wave function assumes the  $5p\sigma$  character.

### V. DIABATIC STATES

Near the equilibrium separation, the states described in the previous section have been charac-

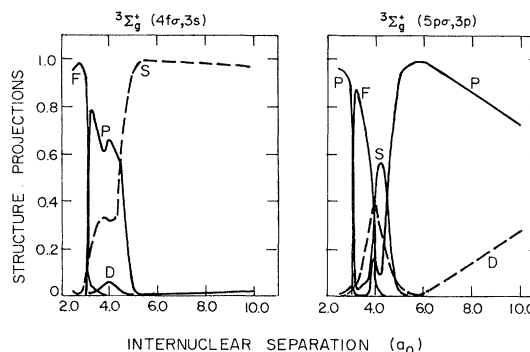


FIG. 5. Cumulative structure projections for the  $(4f\sigma, 3s)$  and  $(5p\sigma, 3p)$   ${}^3\Sigma_g^+$  states of  $\text{He}_2$ .

terized as Rydberg states bound to the  $\text{He}_2^+(^2\Sigma_u^+)$  molecular ion core, i.e., the  $A$  core. Mulliken<sup>9</sup> and others have suggested that similar states could be constructed corresponding to a Rydberg electron bound to the repulsive  $^2\Sigma_g^+$   $B$  core of  $\text{He}_2^+$ . Since these states would be in the continuum, they could not be determined unambiguously by the usual variational methods. However, we do find energies lying in the continuum whose eigenvectors have large contributions from configurations having well-developed  $B$  cores. (Several of the FO and GVB states of Guberman and Goddard's calculations also lie in the continuum.<sup>6</sup>) We have examined the dependence of these energies on our basis sets for  $^3\Sigma_g^+$  states.

We have calculated wave functions and potential curves for  $^3\Sigma_g^+$  states using six-, thirteen-, and seventeen-configuration wave functions. The wave functions for these states are given in Tables III-V. Three configurations in the six-configuration calculation involve  $A$  cores at small  $R$  and have energies lying in the discrete-state region. Likewise, six of the thirteen configurations and nine of the seventeen configurations involve  $A$  cores and energies in the discrete region. Some of the potential curves obtained are shown in Fig. 6. The lowest state of this symmetry, viz.,  $(3p\sigma, 2s)$ , is calculated in all three bases. We show the potential curve of the state to indicate the relative improvement in the energies resulting from the use of the larger basis sets. The change is of the order of  $10^{-3}$  a.u.

The states of interest are, in each basis, the state with the highest bound potential-energy curve and the states corresponding to the next two higher potential curves. In each case, there are  $n$  configurations which develop  $A$  cores and have energies lying in the discrete region. However, there are only  $n - 1$  true bound states produced. In each calculation, the  $n$ th potential curve develops as a normal bound state from large  $R$  to about  $3.125a_0$ . Inside that point, it becomes repulsive and rises into the continuum, crossing the  $\text{He}_2^+$  curve near  $2.88a_0$ . Note that the three potentials for the  $n$ th

TABLE III. Six-term wave function for  $^3\Sigma_g^+$  states.

$\Psi_6 = C_1[1s'_a 2s_a(1s_b 1s_b)] + C_2[1s'_a 2p_{0a}(1s_b 1s_b)]$ $+ C_3[1s'_a 3s_a(1s_b 1s_b)] + C_4[1s'_a 3p_{0a}(1s_b 1s_b)]$ $+ C_5[1s'_a 4s_a(1s_b 1s_b)] + C_6[1s'_a 4p_{0a}(1s_b 1s_b)]$			
Orbital exponents			
1s	1.687	3s	0.320 241
1s'	2.000	3p <sub>0</sub>	0.335 467
2s	0.500	4s	0.265 964
2p <sub>0</sub>	0.550 676	4p <sub>0</sub>	0.358 822

TABLE IV. Thirteen-term wave function for  $^3\Sigma_g^+$  states.

$\Psi_{13} = C_1[1s'_a 2s_a(1s_b 1s_b)] + C_2[1s'_a 2p_{0a}(1s_b 1s_b)]$ $+ C_3[1s'_a 3s_a(1s_b 1s_b)] + C_4[1s'_a 3p_{0a}(1s_b 1s_b)]$ $+ C_5[1s'_a 3d_{0a}(1s_b 1s_b)] + C_6[1s'_a 4s_a(1s_b 1s_b)]$ $+ C_7[1s'_a 4p_{0a}(1s_b 1s_b)] + C_8[1s'_a 4d_{0a}(1s_b 1s_b)]$ $+ C_9[1s'_a 4f_{0a}(1s_b 1s_b)] + C_{10}[1s'_a 5s_a(1s_b 1s_b)]$ $+ C_{11}[1s'_a 5p_{0a}(1s_b 1s_b)] + C_{12}[1s'_a 5d_{0a}(1s_b 1s_b)]$ $+ C_{13}[1s'_a 5f_{0a}(1s_b 1s_b)]$			
Orbital exponents			
1s	1.687	4p <sub>0</sub>	0.358 822
1s'	2.000	4d <sub>0</sub>	0.275
2s	0.309 561	4f	0.250
2p <sub>0</sub>	0.550 676	5s	0.200
3s	0.320 241	5p <sub>0</sub>	0.200
3p <sub>0</sub>	0.335 467	5d <sub>0</sub>	0.200
3d <sub>0</sub>	0.334 027	5f <sub>0</sub>	0.200
4s	0.265 964		

state in each calculation are very similar for small  $R$ . This suggests that the  $n$ th-state wave function does not mix strongly with configurations containing larger orbitals and that it is adequately represented by the configurations used in the six-configuration calculation.

TABLE V. Seventeen-term wave function for  $^3\Sigma_g^+$  states.

$\Psi_{17} = C_1[1s'_a 2s_a(1s_b 1s_b)] + C_2[1s'_a 2p_{0a}(1s_b 1s_b)]$ $+ C_3[1s'_a 3s_a(1s_b 1s_b)] + C_4[1s'_a 3p_{0a}(1s_b 1s_b)]$ $+ C_5[1s'_a 3d_{0a}(1s_b 1s_b)] + C_6[1s'_a 4s_a(1s_b 1s_b)]$ $+ C_7[1s'_a 4p_{0a}(1s_b 1s_b)] + C_8[1s'_a 4d_{0a}(1s_b 1s_b)]$ $+ C_9[1s'_a 4f_{0a}(1s_b 1s_b)] + C_{10}[1s'_a 5s_a(1s_b 1s_b)]$ $+ C_{11}[1s'_a 5p_{0a}(1s_b 1s_b)] + C_{12}[1s'_a 5d_{0a}(1s_b 1s_b)]$ $+ C_{13}[1s'_a 5f_{0a}(1s_b 1s_b)] + C_{14}[1s'_a 5g_{0a}(1s_b 1s_b)]$ $+ C_{15}[1s'_a 6p_{0a}(1s_b 1s_b)] + C_{16}[1s'_a 6f_{0a}(1s_b 1s_b)]$ $+ C_{17}[1s'_a 6h_{0a}(1s_b 1s_b)]$			
Orbital exponents			
1s	1.687	4f <sub>0</sub>	0.250
1s'	2.000	5s	0.200
2s	0.500	5p <sub>0</sub>	0.200
2p <sub>0</sub>	0.550 676	5d <sub>0</sub>	0.200
3s	0.320 241	5f <sub>0</sub>	0.200
3p <sub>0</sub>	0.335 467	5g <sub>0</sub>	0.200
3d <sub>0</sub>	0.334 027	6p <sub>0</sub>	0.1666
4s	0.265 964	6f <sub>0</sub>	0.1666
4p <sub>0</sub>	0.358 822	6h <sub>0</sub>	0.1666
4d <sub>0</sub>	0.275		

We have also calculated potential curves corresponding to configurations based on a pure *A* or *B* core. The configurations used in these wave functions were formed from products of excited STO's on both nuclei and a single-configuration valence-bond representation of the pure *A* or *B*-core state. In Fig. 6, the curve labeled "*B* core" indicates the lowest potential curve obtained from the calculation using only the *B*-core configuration. The lowest continuum *A*-core-state potential is also shown.

The valence-bond wave functions in the crossing region are dominated by configurations containing small excited *s* and *p* orbitals and are similar to the *B*-core wave functions in this region. This and the similarity of the potential curves makes it appear that there exists a diabatic state which crosses the ion curve in this region. Using the ion-core adjustment procedure previously described, we find the energy of the crossing point to be slightly above the energy of the  $3^3D$  atomic state.

## VI. INELASTIC COLLISIONS

### A. $3^3S \rightarrow 2^3P$ excitation transfer

Bennett, Kindlman, and Mercer<sup>2</sup> have measured total inelastic cross sections for a number of excited states of helium. For the  $3^3S$  state, they report a cross section of  $(2.1 \pm 0.5) \times 10^{-16}$  cm<sup>2</sup>. They interpreted their results to mean that a single irreversible collisional-deactivation process was responsible, and they suggested associative ionization. However, Wellenstein and Robertson<sup>1</sup> have since reported  $0.01 \times 10^{-16}$  cm<sup>2</sup> as an upper bound for the associative ionization cross section from the  $3^3S$  state. They also found no measurable cross sections for the endothermic excitation-transfer reactions  $3^3S \rightarrow 3^3P$  and  $3^3S \rightarrow 3^3D$ . However, their upper bound on the total collisional-deactivation cross section was  $8.0 \times 10^{-16}$  cm<sup>2</sup>.

We suggest that the cross section measured by Bennett, Kindlman, and Mercer for the deactivation of  $3^3S$  actually corresponds to the transition  $3^3S \rightarrow 2^3P$ . This is consistent with the results of Wellenstein and Robertson. The absence of a measurable cross section for excitation transfer from  $3^3S$  to a higher  $n=3$  level for thermal collisions is easily understood in terms of energy considerations. In the interaction between a  $3^3S$  and ground-state helium atom only  $\Sigma$  states arise and there is no likely mechanism for excitation transfer among the  $^3\Sigma_g^+$  states since there are no avoided crossings between the  $(4f\sigma, 3s)$  state and lower states. Among the  $^3\Sigma_u^+$  states, however, the interaction between the  $(3d\sigma, 3s)$  and the  $(3s\sigma, 2p)$  states discussed above does seem favorable for excitation transfer. The large energy separation

between the  $2^3P$  and  $3^3S$  states insures irreversibility of the proposed reaction.

We have calculated inelastic cross sections for this transition using the Stueckelberg-Landau-Zener<sup>10</sup> (SLZ) approximation. The interpolated minimum energy separation between the adiabatic potential curves is  $4.9 \times 10^{-4}$  a.u. at  $R=2.71a_0$ . In the two-state approximation, the coupling matrix element equals half the separation of the adiabatic potentials at the position of minimum separation. Dependence on the coupling is illustrated by arbitrarily scaling the matrix element by a parameter  $f$ . Diabatic potential curves were constructed by interpolating between the *ab initio* adiabatic potential curves. The difference of the slopes of the interpolated potentials was 0.0096 a.u.  $a_0^{-1}$ . We believe the SLZ approximation to be valid in this case.<sup>11</sup>

In the description of the  $(3d\sigma, 3s)$  state, we noted the presence of a small barrier in the potential curve. In addition to preventing the  $3^3S \rightarrow 2^3P$  reaction for relative energies much below the peak value, the hump causes the truncation of the par-

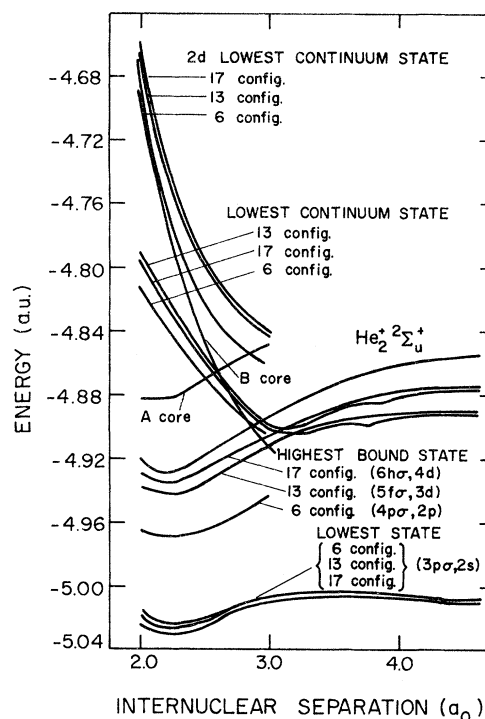


FIG. 6. Comparisons of potential curves obtained from 6-, 13-, and 17-configuration calculations. Curves are given for the highest and lowest bound states and the lowest and second-lowest continuum states. Also shown are the lowest continuum curves obtained in 6-configuration calculations which involve pure *A* and *B* cores, so labeled. The  $^2\Sigma_u^+$  ground-state  $\text{He}_2^+$  curve is also given for comparison.

tial-wave expansion due to the rapid rise of the usual centrifugal barrier in the hump region. We have accounted for quantum-mechanical barrier penetration by multiplying each partial cross section by the appropriate WKB transmission coefficient. In general, only one or two partial waves greater than the largest one allowed classically contributes to the cross sections. This is due more to the width of the barrier rather than its height. The barrier height was taken with respect to the potential at  $R = 15.0a_0$ . This reduces the barrier to  $4 \times 10^{-4}$  a.u. (0.0109 eV). We have also calculated cross sections with the barrier removed. For both cases, the cross sections have been calculated for several values of the interaction matrix element in order to illustrate sensitivity. The results of these calculations are shown in Fig. 7.

There are several general features of these cross sections which are not dependent upon the exact values of the theoretical parameters. The cross sections computed without the barrier in the potential curve rise monotonically as the energy is decreased. When the barrier is introduced into the calculation, the cross sections are reduced due to the exclusion of the larger partial waves for which the Landau-Zener transition probability was the greatest. These results do indicate, however, that experimental studies of the inelastic cross

sections as a function of temperature could be quite useful in determining the height of the barrier. The temperature dependence of the total inelastic cross section for the  $3^1P$  state has recently been studied by Hunter and Leinhardt.<sup>12</sup> They found that the cross section increased at very low temperatures ( $\sim 22^\circ\text{K}$ ). The theoretical description of excitation transfer from the  $3^1P$  level is, however, complex and subject to more uncertainty than the collision processes dealt with here. The relative simplicity of collisional processes originating from the  $3^3S$  or  $3^1S$  states would make the temperature dependence of these states particularly interesting.

### B. $3^3P \rightarrow 3^3S$ excitation transfer

The velocity-averaged cross section for  $3^3P \rightarrow 3^3S$  has also been measured by Wellenstein and Robertson.<sup>1</sup> There does not seem to be a mechanism for this reaction among the ungerade molecular states. In the  $^3\Sigma_g^+$  system, however, there is an avoided crossing between the  $(4f\sigma, 3s)$  and  $(5p\sigma, 3p)$  states near  $4.75a_0$ . The interaction between these two states in this region is probably responsible for this transition. There is another avoided crossing of these same adiabatic states near  $3.0a_0$ . However, the large hump in the  $(5p\sigma, 3p)$  potential near  $3.75a_0$  may prevent transitions occurring in this region from leading to excitation transfer.

### C. Associative ionization

The second collisional process to be considered is associative ionization. The most recent and detailed experimental investigation of this reaction is that of Wellenstein and Robertson.<sup>1</sup> They report associative-ionization cross sections of  $(1.6 \pm 0.1)$  and  $(4.5 \pm 0.5) \times 10^{-16} \text{ cm}^2$ , for the  $3^3P$  and  $3^3D$  states, respectively. They could only place an upper bound of  $0.01 \text{ \AA}^2$  on the cross section for the  $3^3S$  state and suggested that in fact the cross section may be zero. While we are not able to provide a detailed mechanism for this reaction, we can suggest a possible reaction path, and eliminate other states from consideration.

In the previous section we examined several different representations of the repulsive  $^3\Sigma_g^+$  continuum states and found a "stabilized" energy in the vicinity of the crossing point. Guberman and Goddard have reported a  $^1\Sigma_g^+$  state with similar behavior. Our  $^3\Sigma_g^+$  continuum curve, the  $\text{He}_2^+$  ion curve, and the curves corresponding to the three adiabatic states are shown in Fig. 8. All potential curves have been modified by the ion-core adjustment procedure. The continuum potential curve represents an average of the three valence-bond curves shown in Fig. 6. The location of the point

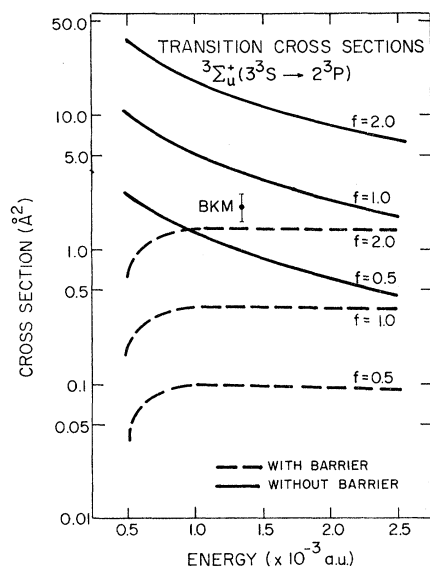


FIG. 7. Total inelastic cross sections for the  $3^3S \rightarrow 2^3P$  transition (via  $^3\Sigma_u^+$  states) calculated within the SLZ approximation are given as a function of energy. Results are illustrated for several values of the coupling-scaling parameter  $f$ , with and without account of the potential barrier. The experimental result of Bennett, Kindlman, and Mercer (Ref. 2) is also shown.

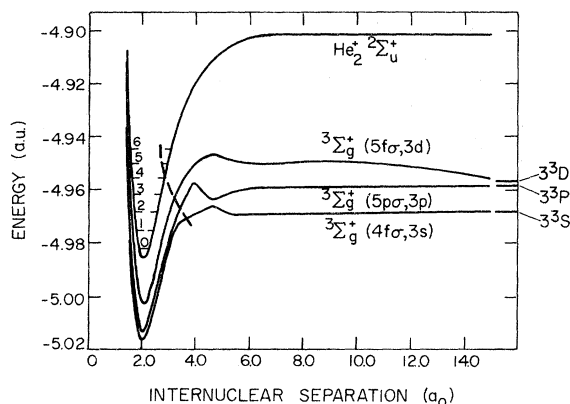


FIG. 8. Possible "diabatic" path (dashed curve) passing through the  $\text{He}_2$  Rydberg-state curves which would provide a mechanism, via avoided crossings, for associative ionization from the  $n=3$  states of He.

at which this curve crosses the ion curve is uncertain by about  $10^{-3}$  a.u. However, the crossing does appear to be in the vicinity of the  $v=4$  vibrational state of the ion.

The Wellenstein-Robertson results<sup>1</sup> indicate that collisions between ground state and both  $3^3P$  and  $3^3D$  excited-state atoms can result in associative ionization at thermal energies. It is clear from the potential curves that the  $(5f\sigma, 3d)$  state cannot be involved in the mechanism at intermediate  $R$ , unless higher configuration interactions greatly reduce the hump. However, this state is mixed with the  $(5p\sigma, 3p)$  state at large  $R$  and this coupling allows transfer to occur from  $(5f\sigma, 3d)$  to  $(5p\sigma, 3p)$ . As  $R$  becomes smaller, the trajectory may be determined by the  $(5p\sigma, 3p)$  adiabatic potential into the region of the peak in the curve at  $4.0a_0$ . In this region it is strongly mixed with other electronic states, in particular  $(4f\sigma, 3s)$ , and eventually with the diabatic state which carries the system into the ionization continuum in the region of  $v=4$ .

In the case of the  $3^3\Sigma_u^+$  states shown in Fig. 1, there is no obvious mechanism for associative ionization involving the  $(3d\sigma, 3s)$  state. The large barrier in the  $(4d\sigma, 3p)$  curve at intermediate  $R$  makes it somewhat unlikely that these states are involved in the associative-ionization mechanism. Nevertheless, if smaller barriers were found in

a more precise calculation, the mechanism indicated for the  $3^3\Sigma_g^+$  states should certainly be considered for the  $3^3\Sigma_u^+$  states as well.

There are a number of other adiabatic states which correlate with the  $3^3D$  and  $3^3P$  atomic states. The potential curves for these states are either included in previous sections or may be inferred from the rules for the behavior of the major configuration-state functions from which these states would be constructed.

Two  $\Delta$  states may be formed from the  $3^3D$  separated atom state. The  $3^3\Delta_u(3d\delta, 3d)$  curve should be purely attractive and would not be expected to interact strongly with any other molecular states of  $3^3\Delta_u$  symmetry, since none lie below it. It may, however, interact with  $3^3\Pi_u$  states through angular coupling terms. This interaction would result in excitation transfer to the  $2^3P$  state, but would *not* be expected to lead to associative ionization. The  $3^3\Delta_g(4f\delta, 3d)$  curve is initially repulsive at intermediate  $R$ , due to the repulsive core, and it probably does not couple strongly with any other molecular state in thermal collisions.

Four  $\Pi$  states arise from the  $3^3P$  and  $3^3D$  atomic states. The  $3^3\Pi_g(3p\pi, 3p)$  curve is purely attractive and should cross the  $3^3\Sigma_g^+(4p\sigma, 2p)$  curve. There may be a small angular coupling between these states which could result in excitation transfer; however, any contribution to associative ionization seems unlikely. The  $3^3\Pi_g(4p\pi, 3d)$  curve should have a hump at intermediate internuclear separations which would prevent its coupling with other states. The  $3^3\Pi_u$  states are shown in Fig. 3. A mechanism for excitation transfer from  $3^3D$  to  $3^3P$  clearly exists. However, the large separation of the  $(4d\pi, 3p)$  state from adjacent states, and the hump present in the  $(5d\pi, 3d)$  curve probably precludes any *direct* contribution to associative ionization.

#### ACKNOWLEDGMENTS

We are grateful to W. A. Goddard for discussions of his work prior to publication and to G. K. Walters for his helpful comments on the published experimental work. We also wish to thank J. S. Cohen for his advice in early stages of the molecular-structure calculations.

\*Supported in part by the U. S. Atomic Energy Commission and the Robert A. Welch Foundation.

†NRC Fellow, now at Johnson Spacecraft Center, Houston, Tex. 77058.

<sup>1</sup>H. F. Wellenstein and W. W. Robertson, *J. Chem. Phys.* **56**, 1072 (1972); **56**, 1077 (1972); **56**, 1411 (1972).

<sup>2</sup>W. R. Bennett, P. J. Kindlman, and G. N. Mercer, *Appl. Opt. Suppl.* **2**, 34 (1965).

<sup>3</sup>B. K. Gupta and F. A. Matsen, *J. Chem. Phys.* **47**, 4860 (1967).

<sup>4</sup>B. Rosen, *Spectroscopic Data Relative to Diatomic Molecules* (Pergamon, Oxford, 1970), p. 193.

- <sup>5</sup>P. N. Reagan, J. C. Browne, and F. A. Matsen, *Phys. Rev.* 132, 304 (1963).
- <sup>6</sup>S. L. Guberman and W. A. Goddard, III, *Chem. Phys. Lett.* 14, 460 (1972); S. L. Guberman, Ph.D. thesis (California Institute of Technology, 1973) (unpublished).
- <sup>7</sup>J. C. Browne, Ph.D. thesis (University of Texas, 1961) (unpublished).
- <sup>8</sup>M. L. Ginter and R. Battino, *J. Chem. Phys.* 52, 9469 (1970).
- <sup>9</sup>R. S. Mulliken, *Phys. Rev.* 136, A962 (1964).
- <sup>10</sup>E. C. G. Stueckelberg, *Helv. Phys. Acta* 5, 369 (1932); L. Landau, *Phys. Z. Sowjetunion* 1, 46 (1934); 1, 88 (1932); C. Zener, *Proc. R. Soc. A* 137, 696 (1932).
- <sup>11</sup>J. S. Cohen, S. A. Evans, and N. F. Lane, *Phys. Rev. A* 4, 2235 (1971).
- <sup>12</sup>W. W. Hunter and T. E. Leinhardt, *J. Chem. Phys.* 58, 941 (1973).